Exp.-Nr. **A2-09/09**
Eingang: 15.05.2009
an PAC: 18.05.2009

Mainz Microtron MAMI

Collaboration A2: "Tagged Photons"
Spokesperson: A. Thomas

Proposal for an Experiment

"Spin observables for $\pi\eta$ photoproduction in the $D_{33}(1700)$ region"

Spokespersons for the Experiment :
V.L. Kashevarov (Lebedev Phisical Institute, Moscow, Ru)
A. Fix (Tomsk Polytechnic University, Tomsk, Ru)
M. Ostrick (Institut für Kernphysik, University of Mainz, D)

Abstract of Physics :

Recently measured total and differential cross sections for the reaction $\gamma p \to \pi^0\eta p$ indicate a dominance of the $\Delta(1700)D_{33}$ resonance in the energy range $E_\gamma = 0.95 - 1.4$ GeV. We propose to make use of this dominance to study systematically properties of the $D_{33}(1700)$ as well as other partial wave amplitudes that reveal themselves via interference with it. Such bilinear combinations of partial wave amplitudes can be extracted by measuring the transverse spin observables T and F.

Abstract of Equipment :

The experiment will be performed at the tagged photon facility of MAMI (Glasgow-Tagger) using the Crystal Ball/TAPS detector setup together with a transversly polarized frozen-spin butanol and circular polarized photon beam.

MAMI Specifications :

beam energy	1558 MeV
beam current	< 100 nA
beam polarisation	polarized

Photon Beam Specifications :

tagged energy range	600 - 1480 MeV
photon beam polarisation	circularly polarized

Equipment Specifications :

detectors	Crystal Ball/TAPS
target	frozen spin butanol (transversly polarized)

Beam Time Request :

set–up/tests with beam	10 hours (parallel with proposal A2-08/09)
data taking	500 hours (parallel with proposal A2-08/09)

List of participating authors:

- **Institut für Physik, University of Basel, Switzerland**
  I. Jaegle, I. Keshelashvili, B. Krusche, Y. Maghrbi, F. Pheron, T. Rostomyan, D. Werthmüller
- **Institut für Experimentalphysik, University of Bochum, Germany**
  W. Meyer, G. Reicherz
- **Helmholtz–Institut für Strahlen- und Kernphysik, University of Bonn, Germany**
  R. Beck, A. Nikolaev
- **Massachusetts Institute of Technology , Cambridge, USA**
  A. Bernstein, W. Deconinck
- **JINR, Dubna, Russia**
  N. Borisov, A. Lazarev, A. Neganov, Yu.A. Usov
- **School of Physics, University of Edinburgh, UK**
  D. Branford, D.I. Glazier, T. Jude, M. Sikora, D.P. Watts
- **Petersburg Nuclear Physics Institute, Gatchina, Russia**
  V. Bekrenev, S. Kruglov, A. Koulbardis
- **Department of Physics and Astronomy, University of Glasgow, UK**
  J.R.M. Annand, D. Hamilton, D. Howdle, K. Livingston, J. Mancell, J.C. McGeorge, I.J.D. MacGregor, E.F. McNicoll, R.O. Owens, J. Robinson, G. Rosner
- **Department of Astronomy and Physics, Saint Mary's University Halifax, Canada**
  A.J. Sarty
- **Kent State University, Kent, USA**
  D.M. Manley
- **University of California, Los Angeles, USA**
  B.M.K. Nefkens, S. Prakhov, A. Starostin, I.M. Suarez
- **MAX-lab, University of Lund, Sweden**
  L. Isaksson
- **Institut für Kernphysik, University of Mainz, Germany**
  P. Aguar-Bartolome, H.J. Arends, S. Bender, A. Denig, E.J. Downie, N. Frömmgen, E. Heid, O. Jahn, H. Ortega, M. Ostrick, B.Oussena, P.B. Otte, S. Schumann, A. Thomas, M. Unverzagt
- **Institut für Physik, University of Mainz, D**
  J.Krimmer, W.Heil
- **University of Massachusetts, Amherst, USA**
  P.Martel, R.Miskimen
- **Institute for Nuclear Research, Moscow, Russia**
  G. Gurevic, R. Kondratiev, V. Lisin, A. Polonski
- **Lebedev Physical Institute, Moscow, Russia**
  S.N. Cherepnya, L.V. Fil'kov, V.L. Kashevarov
- **INFN Sezione di Pavia, Pavia, Italy**
  A. Braghieri, A. Mushkarenkov, P. Pedroni
- **Department of Physics, University of Regina, Canada**
  G.M. Huber
- **Mount Allison University, Sackville, Canada**
  D. Hornidge
- **Tomsk Polytechnic University, Tomsk, Russia**
  A. Fix

- **Physikalisches Institut, University of Tübingen, Germany**
  P. Grabmayr, T. Hehl, D.G. Middleton
- **George Washington University, Washington, USA**
  W. Briscoe, T. Morrison, B.Oussena, B. Taddesse, M. Taragin
- **Catholic University, Washington, USA**
  D. Sober
- **Rudjer Boskovic Institute, Zagreb, Croatia**
  M. Korolija, D. Mekterovic, S. Micanovic, I. Supek

1 Motivation

The spectrum and properties of excited baryons reflect directly the complex non perturbative nature of QCD. At energy scales typical for hadronic masses QCD still lacks exact predictive power. Lattice calculations have provided first encouraging results for ground state properties as well as for the mass spectrum of the lowest excited states. Nevertheless model calculations incorporating partially properties, symmetries or consequences of QCD are indispensable tools to identify the relevant mechanisms responsible for the emergence of excited hadrons and resonance phenomena. Prominent examples are constituent quark models which reproduce main features of the excitation spectrum below 2 GeV (e.g. [1]) or calculations based on unitary extensions of effective-field theories which stress the importance of channel coupling and the dynamical generation of resonances by the strong meson baryon interaction [2, 3, 4, 5]. Moreover, not only the interpretation in terms of QCD but also the empirical knowledge about resonance properties is still rather limited. The results summarised by the PDG [6] are essentially based on a comparison of different partial wave analyses of πN scattering and single meson photoproduction. These analyses have to be confronted with double spin observables which recently became accessible experimentally. In special cases where one partial wave amplitude is dominating the reaction dynamics a model independent analysis becomes much simpler. Well known examples are the P_{33} partial wave which dominates the photoproduction of single pions in the energy region of the $\Delta(1232)$ ground state and the S_{11} partial wave which dominates the η production close to threshold.

Multiple meson photoproduction processes can provide important complementary information. In particular, the reaction $\gamma p \to p\pi^0\eta$ has been proposed and used [7] to search for high mass Δ resonances decaying sequentially into the $\pi\eta N$ final state via an intermediate formation of $\eta\Delta(1232)$ or $\pi S_{11}(1535)$ quasi-two-body systems. The $\eta\Delta(1232)$ system is especially suited to trace back such decay chains because it connects only states with the same isospin, i.e. does not mix between N^* and Δ states.

Theoretically, $\pi^0\eta$ photoproduction has recently been studied within unitary extensions of chiral perturbation theory with coupled channels [5, 8, 9, 10]. In these approaches certain resonances are generated dynamically by interaction of the pseudoscalar meson octet with the ground state baryon multiplets. The $S_{11}(1535)$ and the $\Lambda(1405)$ resonance are frequently discussed as candidates for such quasi-bound states of a meson and a baryon. In calculations including spin 3/2 baryons the $\Delta(1700)D_{33}$ can be interpreted as such a dynamically generated resonance with strong coupling to the $\eta\Delta$ and $K\Sigma^*$ channels. The predicted couplings are much stronger than in simple $SU(3)$ estimates. The πS_{11} channel may be interpreted in terms of a final-state interaction in which the nucleon appearing after Δ decay interacts with the η meson via excitation of the $S_{11}(1535)$ resonance.

Recent cross section data and photon asymmetries for the $\gamma p \to p\pi^0\eta$ reaction [7, 11, 12] suggest indeed a simple dynamics in the photon energy range below 1.5 GeV dominated by the excitation and sequential decay of the $D_{33}(1700)$ resonance. This feature provides an effective method to study in detail the properties of this resonance as well as weaker contributions via interference with it.

2 Previous work

The photoproduction of $\pi^0\eta$ pairs on the proton is quite a new topic in photo-meson physics. In the pioneering work [7, 13] on this reaction, it was used to search for sequential decays of higher-mass Δ states. At lower energies some results for the total cross section have been obtained at the Laboratory of Nuclear Science (LNS), Japan [14]. More recently, cross sections as well as linear beam asymmetries have been measured at the GRAAL facility at ESRF [11], and with the Crystal-Barrel /TAPS detector at ELSA[15].

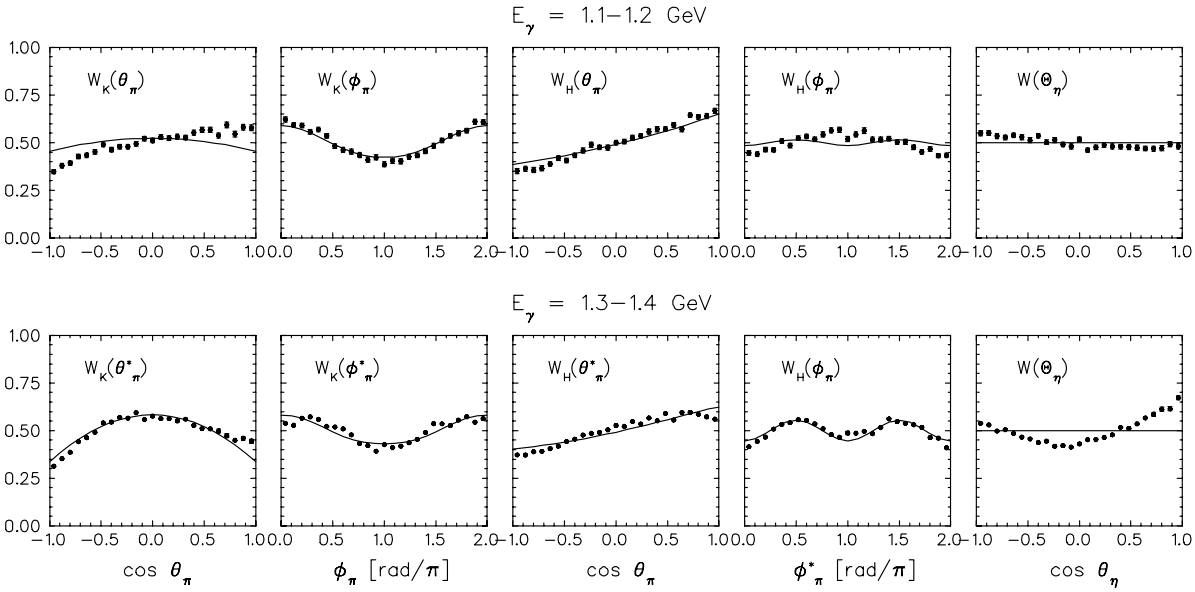

Figure 1: Angular distributions of pions and η mesons in $\gamma p \to \pi^0 \eta p$. The data are corrected for the detector acceptance. The first four panels in each row are distributions of pions calculated in πp c.m. frame. The notations W_K and W_H are related to the canonical and helicity systems, whose meaning is explained in ref. [12, 16]. The last panels present angular distribution of η-mesons in the overall c.m. system of the reaction. The curves are results from a model calculation including only the $D_{33}(1700)$.

An analysis of the experimental results of Horn *et al.* and Ajaka *et al.* [7, 11] together with the theoretical work of Doring *et al.* [5] has shown that in the low-energy region the process is mainly governed by the excitation of the $D_{33}(1700)$ resonance, which decays into the $\pi\eta N$ final state via an intermediate formation of $\eta\Delta(1232)$ or $\pi S_{11}(1535)$ quasi-two-body systems. At higher energies, according to the results of Horn *et al.* [7], other resonances as well as the $pa_0(980)$ configuration start to come into play. Three independent features of the data obtained in [12] indicate the dominance of the D_{33} partial wave amplitude. Firstly, the measured angular distributions do not show any significant variation as function of energy in the region between $E_\gamma = 1.1$ and 1.4 GeV, thus pointing to the dominance of a single partial wave amplitude. A simple phenomenological model including only the D_{33} partial wave appears to be surprisingly successful in describing the measured angular distributions (see Fig. 1), whereas other quantum numbers fail. Secondly, the observed rapid rise of the total cross section at threshold together with almost isotropic angular distribution of η mesons (right panels in Fig. 1) indicates that $\eta\Delta$ system is mostly in an s-state. Finally, the $\pi^0 p$ invariant mass distribution shows the importance of the s-waves in the $\eta\Delta$ systems, thus pointing to the dominance of D_{33}, which is the only partial wave where $\eta\Delta$ system can be produced in a relative s-wave. It is also worth noting that the background contributions are small [5, 16] indicating resonant saturation of $\pi^0\eta$ photoproduction.

The dominance of $D_{33}(1700)$ is a very important result by itself. It implies that apart from the (γ, π^0) and (γ, η) reactions determined respectively by the $\Delta(1232)$ and $S_{11}(1535)$ formation we have another process, $(\gamma, \pi^0\eta)$, whose amplitude in a wide energy range is mainly governed by a single dynamical mechanism, the excitation of $D_{33}(1700)$.

3 Open questions

After the dominance of $D_{33}(1700)$ is established, it is encouraging to study systematically contributions beyond the single D_{33} picture. As was pointed out in [12] the angular distributions while being qualitatively well described by the D_{33} alone, exhibit some deviations from this simple model (see Fig. 1). According to the results of quark models additional contributions may come from the excitation of $P_{33}(1600)$, $P_{31}(1750)$, and $F_{35}(1905)$, decaying into p-wave $\eta\Delta$ state. The admixture of p-waves in $\eta\Delta$ is also born out by a visible forward-backward asymmetry in the distribution over $\cos\Theta_\eta$ in the overall c.m. frame (see right panels in Fig. 1). The p-wave contribution is partly composed of the background terms. However according to the calculation of ref. [16] the role of the background amplitudes is quite insignificant at all energies within region considered (see Fig. 3 in [5]).

One can make a rough estimate of the contribution of various Δ resonances to the reaction taking their parameters from the PDG listing [6]. Neglecting background and using unitarity one arrives at

$$\sigma \approx \sum_R \frac{\pi}{\omega_\gamma^2}(2J+1)\frac{M_R^2\Gamma_{\pi\eta N}(W)\Gamma_{\gamma N}(W)}{(W^2-M_R^2)^2+M_R^2\Gamma_{tot}^2(W)}\,, \tag{1}$$

with ω_γ being c.m. photon energy and M_R denoting the resonance mass. The cross section predicted by the formula (1) is plotted in Fig. 2 together with contributions of the individual resonances. For the partial decay widths in the $\pi^0\eta N$ channel we used the common relation $\Gamma_{\pi\eta N}(M_R) = 0.1\,\Gamma_{tot}(M_R)$ for all states. Although this estimate is very rough because of uncertainties in the partial widths $\Gamma_{\pi\eta N}$, one can expect that $P_{33}(1600)$ resonance can visibly contribute near threshold, whereas $P_{31}(1750)$ and $F_{35}(1905)$ are expected to come into play at higher energies.

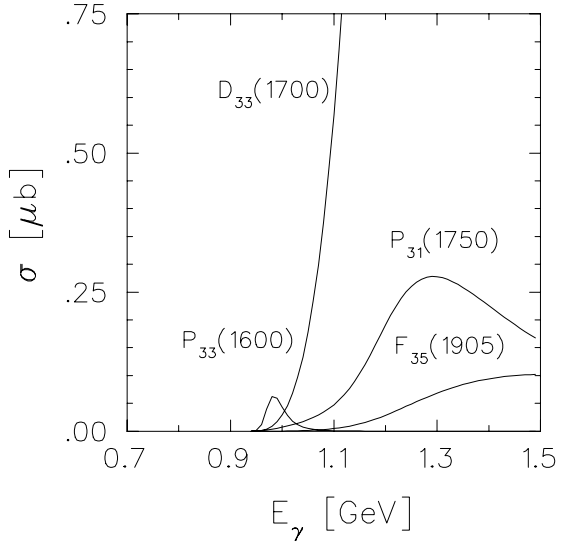

Figure 2: Estimate of resonance contributions to $\gamma N \to \pi^0\eta N$ calculated using the formula (1). For the electromagnetic and hadronic decay widths the values from the PDG compilation [6] are taken. For the partial widths $\Gamma_{\pi\eta N}$ the same values $\Gamma_{\pi\eta N} = 0.1\,\Gamma_{tot}$ are used.

At the same time, the estimations in Fig. 2 show that as long as only the total cross section is exploited, there might be much variation in the model parameters of the 'weaker' resonances, which however will fit the total cross section equally well. In such a situation with one strongly dominating partial wave (in our case D_{33}), the contribution of weaker resonances may reveal themselves via interference with this dominant resonance. The interference terms may be isolated via studying polarization observables.

We propose to address properties of the $D_{33}(1700)$ resonance and interference terms with other partial wave amplitudes by measuring spin observables. This will be discussed in the next chapter in more detail.

Due to isospin conservation, the $\eta\Delta$ configuration may be produced only via transition to isospin 3/2 states. However, one can expect that the resonances with $T = 1/2$ may contribute to the reaction as well, emitting $\pi\eta$ via intermediate production of the $\pi S_{11}(1535)$ configuration. The possible importance of the $T = 1/2$ states was pointed out in [12], where the distributions of $\pi^0 p$ invariant mass has been considered. In this connection, another question that has to be addressed is the determination of the isotopic structure of the reaction amplitude by studying other charge channels, namely $\gamma n \to \pi^0\eta n$ and $\gamma p \to \pi^+\eta n$. This point is not included in the present proposal and will be addressed after already existing data with hydrogen and deuterium target have been analysed.

4 Polarization Observables and Proposed Measurements

A general analysis allowing the determination of the moduli and relative phases of the four independent photoproduction amplitudes requires a complete set of polarization experiments, which for photoproduction of two pseudoscalar mesons is discussed, e.g., in [17]. However, in the $\pi\eta$ case, due to dominance of the D_{33} wave, the information on bilinear combinations of the amplitudes will require much less parameters. The situation is similar to that existing in η photoproduction, which is known to be dominated by the S_{11} wave in a wide energy region. Making use of this fact allowed an almost model independent extraction of parameters for the resonance $D_{13}(1520)$ in much cleaner way than in π-photoproduction where it overlaps with many other resonant states.

As follows from the estimation in Fig. 2 in the energy region below $E_\gamma = 1.5$ GeV the main contribution beyond the $D_{33}(1700)$ can be expected to come from the states P_{33} and P_{31}, which would decay into $\eta\Delta$ in a relative p-wave. As the D_{33} decays into a s-wave $\eta\Delta$ state the pure D_{33} model (only a D_{33} amplitude is included) all initial state spin observables (except E) vanish. Therefore, the results of polarization measurements will be sensitive to even small admixture of other resonances.

Since we are not interested in the spin states of the final nucleon it is convenient to present the observables directly in terms of the quadratic forms integrated over the solid angle in the πN c.m. system

$$\sigma_{\lambda\lambda'}(\theta_\eta, \omega_\eta) = \int \sum_{m_f} t^*_{m_f\lambda'}(\theta_\eta, \omega_\eta; \Omega_{\pi N})\; t_{m_f\lambda}(\theta_\eta, \omega_\eta; \Omega_{\pi N})\, d\Omega_{\pi N}\,, \tag{2}$$

where $\lambda = \pm 1/2, \pm 3/2$ and $m_f = \pm 1/2$ are the helicities in the initial and the final states. Then for the individual observables we obtain:

$$\frac{d\sigma^0}{d\Omega} = \frac{1}{2}\left(\sigma_{\frac{1}{2}\frac{1}{2}} + \sigma_{\frac{3}{2}\frac{3}{2}}\right), \quad T\frac{d\sigma^0}{d\Omega} = -\Im m\sigma_{\frac{3}{2}\frac{1}{2}}\,, \tag{3}$$

$$E\frac{d\sigma^0}{d\Omega} = \frac{1}{2}\left(\sigma_{\frac{1}{2}\frac{1}{2}} - \sigma_{\frac{3}{2}\frac{3}{2}}\right), \quad F\frac{d\sigma^0}{d\Omega} = \Re e\,\sigma_{\frac{3}{2}\frac{1}{2}}\,. \tag{4}$$

Predictions for $d\sigma/d\Omega$, E T, and F obtained within the model described in [16] are presented in Fig. 3. The resonance parameters are the same as those used in Fig. 2 and both decay channels, $\eta\Delta$ and πS_{11}, are included.

To understand the main features of the observables more directly we can neglect the πS_{11} channel. Then it is straightforward to obtain the following analytical expressions for the single

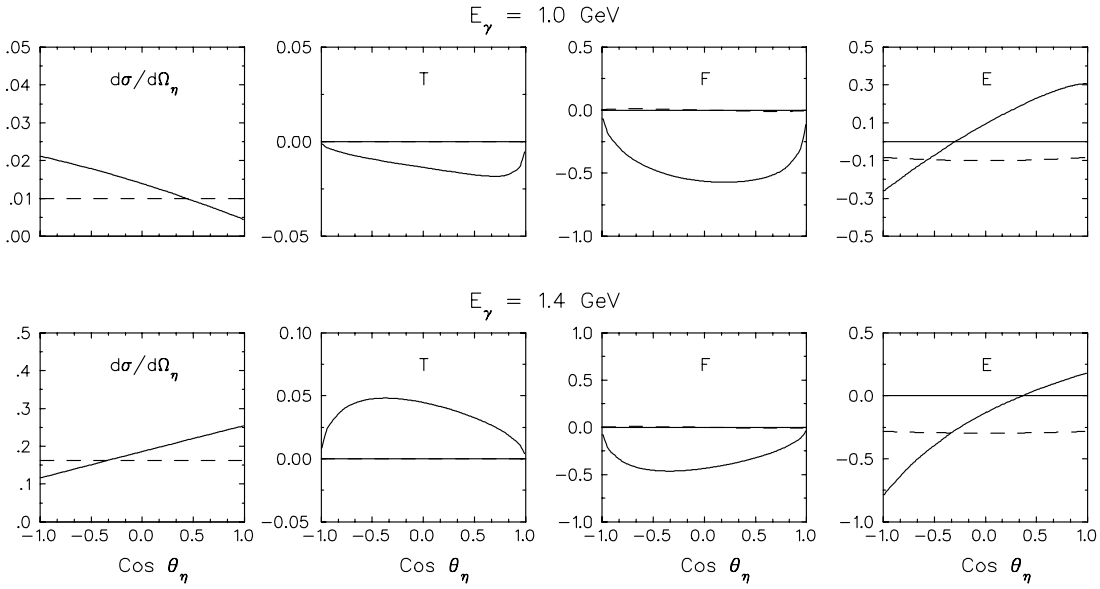

Figure 3: Model calculation of some observables for $\gamma N \to \pi^0\eta N$ at two photon energies. The dashed lines are obtained with $D_{33}(1700)$, whereas the solid lines include contribution from $P_{33}(1640)$ in the upper panels and from $P_{31}(1750)$ in the lower panels.

D_{33} case as well as for the combinations of D_{33} with P_{31} and P_{33} partial wave amplitudes

$$D_{33} \quad : \quad \frac{d\sigma^0}{d\Omega} = A\,, \quad T\frac{d\sigma^0}{d\Omega} \;=\; F\frac{d\sigma^0}{d\Omega} \;=\; 0 \tag{5}$$

$$D_{33}+P_{31} \quad : \quad \frac{d\sigma^0}{d\Omega} \sim 1 + B\cos\theta_\eta\,, \quad T\frac{d\sigma^0}{d\Omega} \sim \sin\theta_\eta\,,\; F\frac{d\sigma^0}{d\Omega} \sim \sin\theta_\eta \tag{6}$$

$$D_{33}+P_{33} \quad : \quad \frac{d\sigma^0}{d\Omega} \sim 1 + C\cos\theta_\eta\,, \quad T\frac{d\sigma^0}{d\Omega} \sim \sin\theta_\eta\,,\; F\frac{d\sigma^0}{d\Omega} \sim \sin\theta_\eta(1+D\cos\theta_\eta) \tag{7}$$

where the constants A, B, C, D are independent of the angle θ_η.

After inclusion of P_{31} or P_{33} partial waves the unpolarized cross section exhibits a characteristic p-wave forward-backward asymmetry with linear dependence on $\cos\theta_\eta$. The pure D_{33} model predicts the transverse spin observables T and F to be comparable with zero. The inclusion of a P_{31} or a P_{33} resonance leads to a characteristic angular dependence. The observable E (longitudinally polarized target) turns out to be almost angular independent and is approximately equal to

$$E \approx \frac{1-a}{1+a}\,, \quad a = \left(\frac{A_{3/2}}{A_{1/2}}\right)^2 \tag{8}$$

where A_λ is helicity amplitude of the transition $\gamma N \to D_{33}$. This value also influences the unpolarised cross section. In our analysis [12] values for a in the range from 0.7 and 1.45 were obtained depending on the energy. In contrast to the single pseudoscalar meson photoproduction E does not equal to 1 at $\theta_\eta = 0$ and $\theta_\eta = \pi$. The reason lies in the spin 3/2 of the Δ resonance, so that azimuthal asymmetry at $\theta_\eta = 0(\pi)$ does not require $\lambda = 1/2$, as in the case of single meson. Inclusion of P_{31} and P_{33} results in strong interference with the leading partial wave, which appears to be negative at forward angles. We do not include a measurement of E in this proposal since a determination of the parameter a is also possible with precisely measured angular distributions. However, it will be possible to obtain results for E using data that will be taken for proposal A2-06/09.

5 Experimental issues

We propose to measure the transverse spin asymmetries T and F for the reaction $\vec{\gamma}\vec{p} \to p\eta\pi^0$ simultaneously using a transversely polarized proton target and a circularly polarized photon beam. For the measurement of T the we will average over the helicity states of the photon beam.

The experiment will be performed at the tagged photon facility of the MAMI C accelerator in Mainz. We will use the maximum energy of MAMI C which is presently $E_0 = 1558$ MeV and will cover the full energy region from the threshold of the $\gamma p \to p\pi\eta$ reaction at $E_{thr} = 930$ MeV up to 95% of E_0 with circularly polarised tagged photons. Polarization degrees higher than 50% will be achieved above 930 MeV incident photon energy. Details are described in appendix A.1.

To detect the all particles in the final state, we will use the hermetic Crystal-Ball/TAPS detector setup (see appendix A.3). The experiment requires transversely polarized protons, which will be provided by a frozen-spin butanol (C_4H_9OH) target constructed in Dubna and Mainz. Also here a more detailed description can be found in the appendix A.2.

The trigger for the DAQ system will be derived from the total energy deposit in the calorimeter distributed over 2 or more clusters ($E_{tot} > 350$ MeV). These conditions have been successfully applied in previous runs with unpolarized hydrogen target and will allow to measure single eta photoproduction in parallel.

The $\gamma p \to p\eta\pi^0$ reaction can be identified using invariant and missing mass techniques as demonstrated in [12]. In the first step events with 4 neutral and 1 or 0 charged particles in the Crystal Ball and TAPS detectors are selected. The π^0 and η mesons are then identified via their decay into 2 photons. The distribution of the invariant masses calculated from possible $\gamma\gamma$ combinations is shown in Fig. 4.

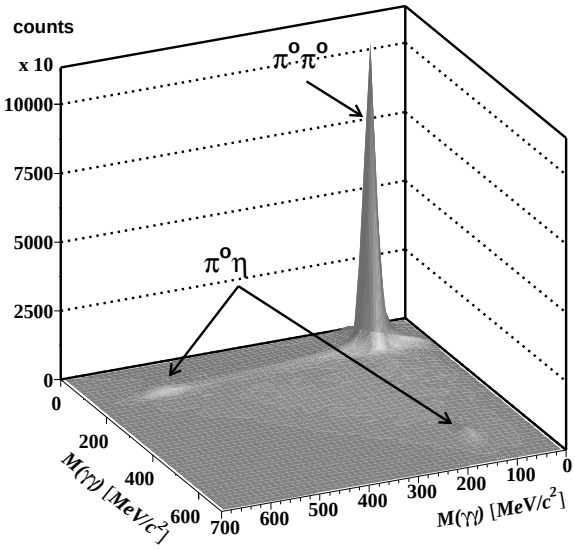

Figure 4: Event selection for final states with 4 photons: $M_{\gamma\gamma}$ *vs* $M_{\gamma\gamma}$ for all possible independent combinations of $\gamma\gamma$ pairs (3 entries for each event).

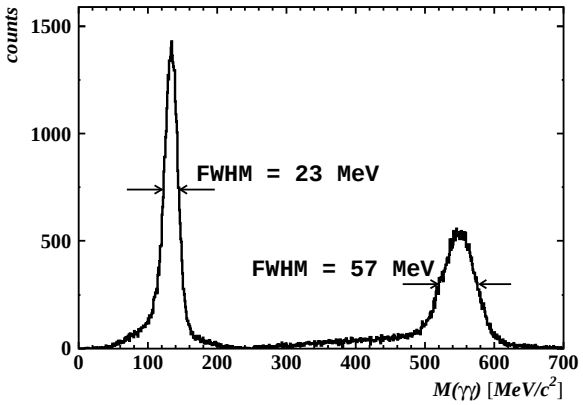

Figure 5: The $\gamma\gamma$ invariant mass spectrum for the best combination of the $\gamma\gamma$ pairs after χ^2 minimization and rejection of $\pi^0\pi^0$ events. One pair corresponds to the $\pi^0 \to \gamma\gamma$ (left), the other to the $\eta \to \gamma\gamma$ decay (right).

As there are 3 independent combinations for such pairs, this histogram has 3 entries per event. The distribution shows a large peak corresponding to the $\pi^0\pi^0$ channel and two smaller ones due to the $\pi^0\eta$ final state. In the next step the χ^2 for each of the two-meson final states,

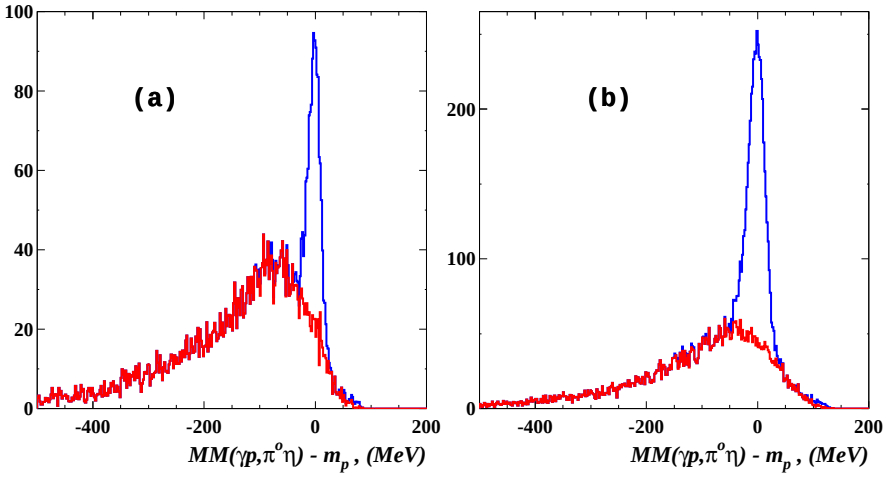

Figure 6: Expected missing mass spectra. (a) $E_\gamma = 1.0 - 1.1 GeV$; (b) $E_\gamma = 1.1 - 1.2 GeV$. Red line - background contribution from ^{12}C and ^{16}O. Blue peak corresponds to the investigated reaction.

$\pi^0\pi^0$ and $\pi^0\eta$, was calculated for the possible combinations:

$$\chi^2_{2\pi} = \left(\frac{M_{\gamma_i\gamma_j} - m_{\pi^0}}{\sigma_{\pi^0}}\right)^2 + \left(\frac{M_{\gamma_k\gamma_l} - m_{\pi^0}}{\sigma_{\pi^0}}\right)^2, \quad (9)$$

$$\chi^2_{\pi\eta} = \left(\frac{M_{\gamma_i\gamma_j} - m_{\pi^0}}{\sigma_{\pi^0}}\right)^2 + \left(\frac{M_{\gamma_k\gamma_l} - m_{\eta}}{\sigma_{\eta}}\right)^2. \quad (10)$$

Here m_{π^0} and m_η are π^0 and η masses and $\sigma_{\pi^0} = 10$ MeV and $\sigma_\eta = 25$ MeV are the corresponding invariant mass resolutions of the detector system (Fig. 5). Each event is now assigned to either $\pi^0\pi^0$ or $\pi^0\eta$ production depending on the minimum of the χ^2 values. After this selection and a rejection of $\pi^0\pi^0$ events the $\gamma p \to \pi^0\eta p$ reaction can be clearly identified on top of a small background (Fig. 5). This histogram has two entries for each event corresponding to the two photon pairs. After applying a $\chi^2_{\pi\eta} < 9$ cut to the two-dimensional $\gamma\gamma$ invariant mass distribution, the residual background can be eliminated by calculating the missing mass. At lower energies there is substantial background $(30-60\%)$, mainly from the $\gamma p \to \pi^0\pi^0 p$ reaction that has a three orders of magnitude higher cross section. This contribution drops rapidly with increasing energy and is reduced to only $\sim 12\%$ for $E_\gamma > 1.2$ GeV.

Using the butanol target has an essential disadvantage because of additional background from reactions on ^{12}C and ^{16}O . In order to estimate this background we have analysed data taken with a carbon target in June 2008 using the same analysis procedure as for runs with a LH_2 target. After normalization of the photon flux and taking into account the number of ^{12}C nuclei in a carbon target with respect to butanol we obtain missing mass spectra that we expect for the proposed experiment (see Fig. 6).

6 Event rates and beamtime estimate

For the measurement of the differential cross section and the double polarization observables F and T we will divide the photon beam energy into 50 MeV wide intervals.

We aim at a statistical precision of δF_{stat}=0.15 in 10 the angular intervals of $cos\Theta_\eta$. For the rate estimate we use a total cross section of σ=1μb. The necessary beam time can be calculated

from

$$\Delta t = \eta[P^2 \delta^2_{stat} \cdot N_\gamma \cdot N_T \cdot \epsilon \cdot b \cdot \Delta\sigma_o]^{-1} \tag{11}$$

with the following notation:

- δ_{stat}: statistical uncertainty of $F \Rightarrow$ **0.15**
- N_γ: number of photons per 50 MeV incident photon energy $\Rightarrow$ $\mathbf{8 \cdot 10^5 sec^{-1}}$
- N_T: surface density of target nuclei (2 cm frozen butanol target) $\Rightarrow$ $\mathbf{0.09\ b^{-1}}$
- ϵ: detection efficiency, assumed on average as $\Rightarrow$ **0.2**
- b: decay branching ratio of η mesons, for $\eta \to 2\gamma \Rightarrow$ **0.4**
- $\Delta\sigma_o$: unpolarized cross section in the respective angular bins.
  We assume minimal $\Rightarrow$ $\Delta\sigma_o$**=0.1** μ**b**
- P: product of polarization degrees $\Rightarrow$ $P_t \cdot P_b$**= 0.6×0.5=0.3**
- $\eta = 1 + B + C$ effective dilution from unpolarized background $\Rightarrow$ **2.0**

With these numbers we arrive at a beam time estimate of

500 hours

A Experimental apparatus

A.1 Photon Beam

The A2 photon beam is derived from the production of Bremsstrahlung photons during the passage of the MAMI electron beam through a thin radiator. The resulting photons can be circularly polarised, with the application of a polarised electron beam, or linearly polarised, in the case of a crystalline radiator. The degree of circular photon polarisation achieved is dependent on the electron beam polarisation ($P_e = 85\%$) and the helicity transfer during the bremsstrahlung process shown in Fig. 7. The Glasgow Photon Tagger (Fig 8) provides energy tagging of the photons by detecting the post-radiating electrons and can determine the photon energy with a resolution of 2 to 4 MeV depending on the incident beam energy, with a single-counter time resolution $\sigma_t = 0.117$ ns [18]. Each counter can operate reliably to a rate of ∼1 MHz, giving a photon flux of $2.5 \cdot 10^5$ photons per MeV. Photons can be tagged in the momentum range from 4.7 to 93.0% of E_0.

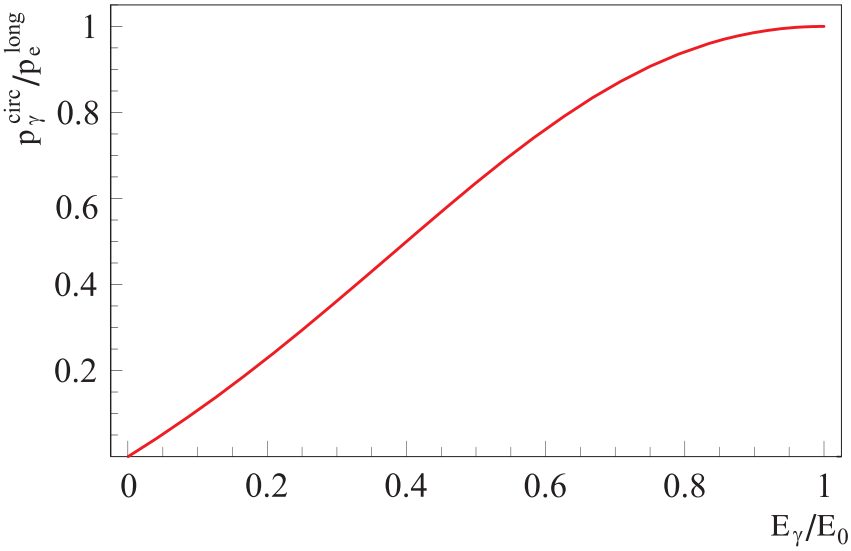

Figure 7: Helicity transfer from the electron to the photon beam as function of the energy transfer. The MAMI beam polarisation is P_e ≈85%.

To augment the standard focal plane detector system and make use of the Tagger's intrinsic energy resolution of 0.4 MeV (FWHM), there exists a scintillating fibre detector ('Tagger Microscope') that can improve the energy resolution by a factor of about 6 for a ∼100 MeV wide region of the focal plane (dependent on its position) [19].

A.2 Frozen-Spin Target

Polarisation experiments using high density solid-state targets in combination with tagged photon beams can reach the highest luminosities. For the double polarisation measurements planned with the Crystal Ball detector on polarised protons and deuterons a specially designed, large horizontal ^{3}He/^{4}He dilution refrigerator was built in cooperation with the Joint Institute for Nuclear Research (JINR) Dubna (see Figure 9). It has minimum limitations for the particle detection and fits into the central core of the inner Particle Identification Detector (PID2). This was achieved by using the frozen spin technique with the new concept of placing a thin superconducting holding coil inside the polarisation refrigerator. Longitudinal and transverse polarisations will be possible.

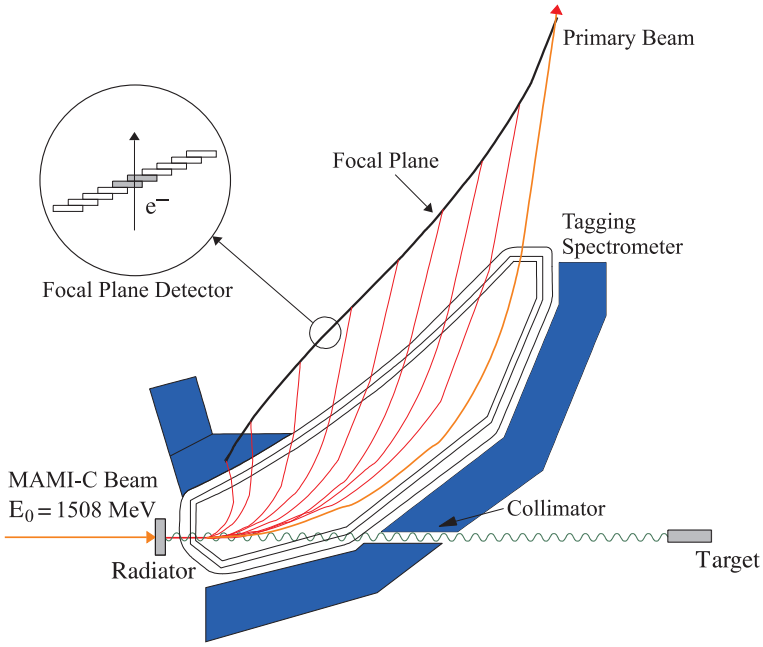

Figure 8: The Glasgow photon tagging spectrometer.

Figure 9: The new dilution refrigerator for the Crystal Ball Frozen Spin Target.

Highest nucleon polarisation in solid-state target materials is obtained by a microwave pumping process, known as 'Dynamic Nucleon Polarisation' (DNP). This process is applicable to any nucleus with spin and has already been used in different experiments with polarised proton and deuteron targets. The geometric configuration of the target is the same for the polarised proton and neutron setup. However, since the polarisation measurement of the deuteron is more delicate due to the small size of the polarisation signals, the modification of some basic components is needed. The reason for this is twofold: firstly the magnetic moment of the deuteron is smaller than that of the proton and, in addition, the interaction of the deuteron quadrupole moment with the electric field gradient in the sample broadens the deuteron polarisation signal. An accuracy $\delta P_p/P_p$ of 2 to 3% for the protons and $\delta P_D/P_D$ of 4 to 5% for the deuterons is expected in the polarisation measurement. It has also to be taken into account that the measured deuteron polarisation P_D is not equal to the neutron polarisation P_n. Assuming a 6 % admixture of the D-state of the deuteron, a calculation based on the Clebsch-Gordon coefficients leads to $P_n = 0.91\ P_D$. Several polarised proton and deuteron materials are available such as alcohols and deuterated alcohols (e.g. butanol C_4H_9OH), NH_3, ND_3 or ^{6}LiD. The most important criteria in the choice of material suitable for particle physics experiments are the degree of polarisation P and the ratio k of free polarisable nucleons to the total number of nucleons. Further requirements on polarised target materials are a short polarisation build-up time and a simple, reproducible target preparation. The polarisation resistance against radiation damage is not an issue for experiments with a low intensity tagged photon beam ($\dot{N}_\gamma \approx 5 \cdot 10^7\ \mathrm{s}^{-1}$) as will be used here. However, the limitations of a reduced relaxation time due to overheating of the target beads (Kapitza resistance) will have to be investigated.

Taking all properties together, butanol and deuterated butanol are the best material for this experiment. For protons we expect a maximum polarisation of $P_p = 90\%$ and an average polarisation of $P_p = 70\%$ in the frozen spin mode. Recently, a deuteron polarisation $P_D = 80\%$ was obtained with Trityl doped butanol targets at 2.5 T magnetic field in a ^{3}He/^{4}He dilution refrigerator. At a 0.4 T holding field an average neutron polarisation P_n (see above) of 50 % will be obtained. The filling factor for the ∼2 mm diameter butanol spheres into the 2 cm long, 2 cm diameter target container will be around 60%. The experience from the GDH runs in 1998 [20] shows that, with a total tagged photon flux of $5 \cdot 10^7$, relaxation times of about 200 hours can be expected. The polarisation has to be refreshed by microwave pumping every two days.

In conclusion, we estimate that we will achieve the following target parameters:

- Maximum total tagged photon flux in the energy range of 4.7 to 93% of E_0: $\dot{N}_\gamma \approx 5 \cdot 10^7 \mathrm{s}^{-1}$, with relaxation time of 200 hours.
- Target proton density in 2 cm cell: $N_T \approx 9.1 \cdot 10^{22} \mathrm{cm}^{-2}$ (including dilution and filling factors)
- Average proton polarisation $P_p = 70\%$
- Target deuteron density in 2cm cell: $N_T \approx 9.4 \cdot 10^{22} \mathrm{cm}^{-2}$ (including dilution and filling factors)
- Average neutron polarisation $P_n = 50\%$

A.3 Crystal Ball/TAPS detector system

The central detector system consists of the Crystal Ball calorimeter combined with a barrel of scintillation counters for particle identification and two coaxial multiwire proportional counters for charged particle tracking. This central system provides position, energy and timing information for both charged and neutral particles in the region between 21° and 159° in the polar angle (θ) and over almost the full azimuthal (ϕ) range. At forward angles, less than 21°, reaction

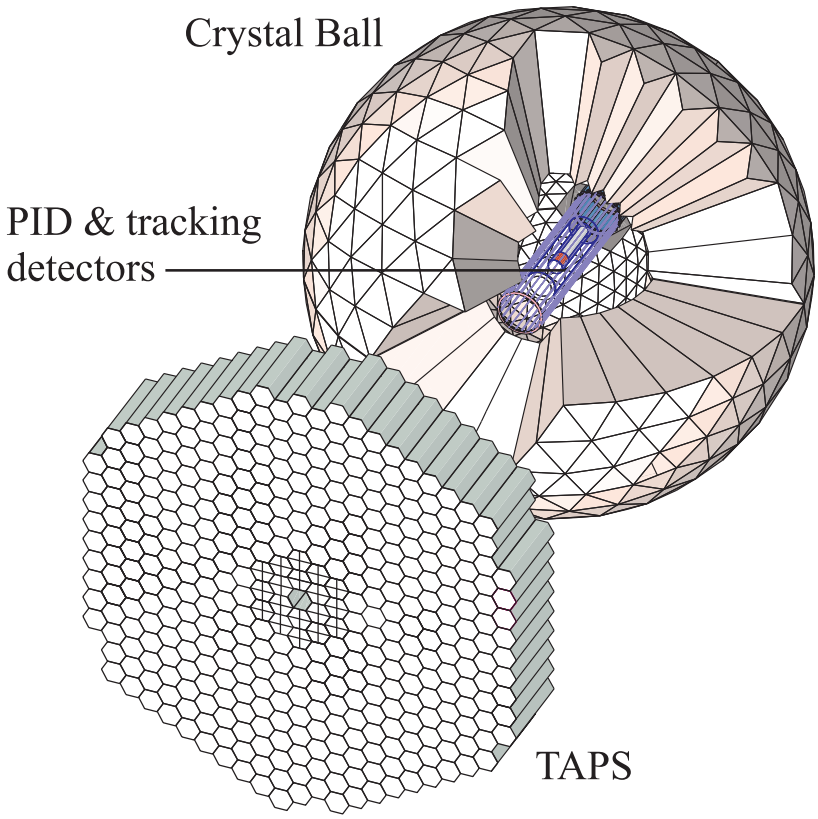

Figure 10: The A2 detector setup: The Crystal Ball calorimeter, with cut-away section showing the inner detectors, and the TAPS forward wall.

products are detected in the TAPS forward wall. The full, almost hermetic, detector system is shown schematically in Fig. 10 and the measured two-photon invariant mass spectrum is shown in Fig. 11.

The Crystal Ball detector (CB) is a highly segmented 672-element NaI(Tl), self triggering photon spectrometer constructed at SLAC in the 1970's. Each element is a truncated triangular pyramid, 41 cm (15.7 radiation lengths) long. The Crystal Ball has an energy resolution of $\Delta E/E = 0.020 \cdot E[GeV]^{0.36}$, angular resolutions of $\sigma_\theta = 2 \ldots 3^\circ$ and $\sigma_\phi = \sigma_\theta / \sin\theta$ for electromagnetic showers [21]. The readout electronics for the Crystal Ball were completely renewed in 2003, and it now is fully equipped with SADCs which allow for the full sampling of pulse-shape element by element. In normal operation, the onboard summing capacity of these ADCs is used to enable dynamic pedestal subtraction and the provision of pedestal, signal and tail values for each element event-by-event. Each CB element is also newly equipped with multi-hit CATCH TDCs. The readout of the CB is effected in such a way as to allow for flexible triggering algorithms. There is an analogue sum of all ADCs, allowing for a total energy trigger, and also an OR of groups of sixteen crystals to allow for a hit-multiplicity second-level trigger - ideal for use when searching for high multiplicity final states.

In order to distinguish between neutral and charged particles species detected by the Crystal Ball, the system is equipped with PID2, a barrel detector of twenty-four 50 mm long, 4 mm thick scintillators, arranged so that each PID2 scintillator subtends an angle of 15° in ϕ. By matching a hit in the PID2 with a corresponding hit in the CB, it is possible to use the locus of the $\Delta E, E$ combination to identify the particle species (Fig. 12). This is primarily used for the separation of charged pions, electrons and protons. The PID2 covers from 15° to 159° in θ.

The excellent CB position resolution for photons stems from the fact that a given photon

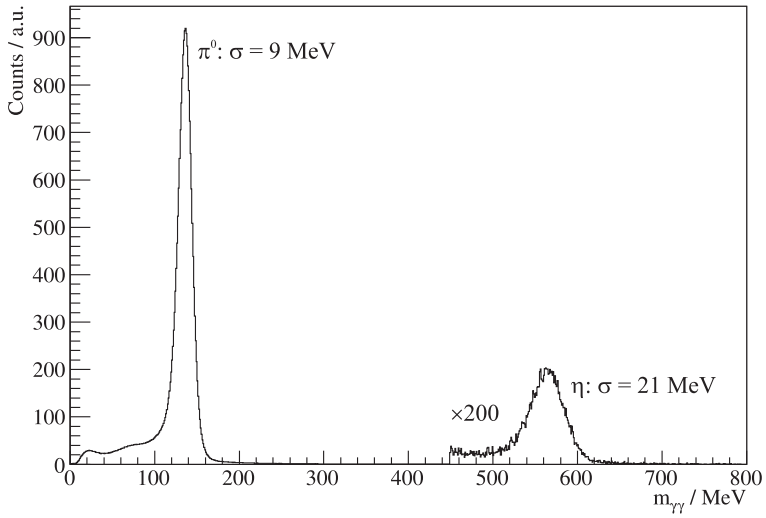

Figure 11: Two photon invariant mass spectrum for the CB/TAPS detector setup. Both η and π^0 mesons can be clearly seen.

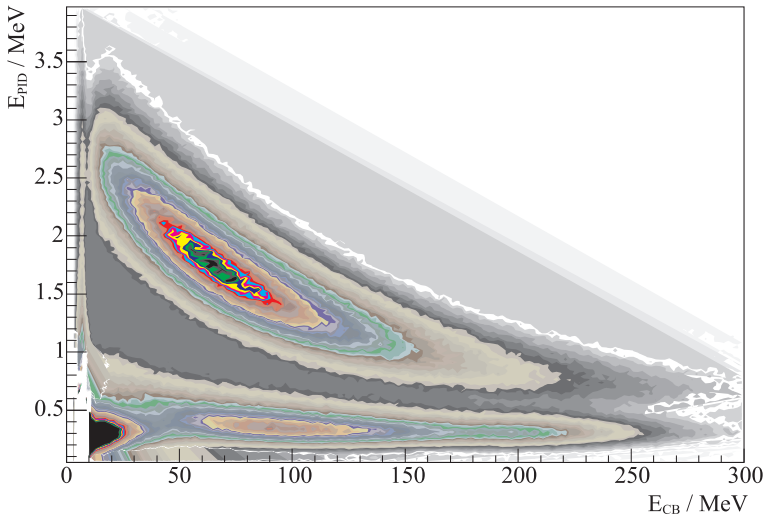

Figure 12: A typical $\Delta E/E$ plot from the Crystal Ball and the PID2 detector. The upper curved region is the proton locus, the lower region contains the pions and the peak towards the origin contains mostly electrons.

triggers several crystals and the energy-weighted mean of their positions locates the photon position to better than the crystal pitch. For charged particles which deposit their energy over only one or two crystals, this is not so precise. Here the tracks of charged particles emitted within the angular and momentum acceptance of the CB detector will be reconstructed from the coordinates of point of intersections of the tracks with two coaxial cylindrical multiwire proportional chambers (MWPCs) with cathode strip readout. These MWPCs are similar to those installed inside the CB during the first round of MAMI-B runs [22]. The most significant difference is that all detector signals are taken at the upstream end of the MWPCs, minimising the material required and facilitating particle detection in the forward polar region.

A mixture of argon (79.5%), ethane (30%) and freon-CF_4 (0.5%) is used as the filling gas. This mixture is a compromise between charge multiplication and localization requirements imposed by the ionizing particle tracks.

Within each chamber both the azimuthal and the longitudinal coordinates of the avalanche will be evaluated from the centroid of the charge distribution induced on the cathode strips. The location of the hit wires(s) will be used to resolve ambiguities which arise from the fact that each pair of inner and outer strip cross each other twice. The expected angular resolution (rms) will be $\sim 2^\circ$ in the polar emission angle θ and $\sim 3^\circ$ in the azimuthal emission angle ϕ.

The MWPCs have been recently installed inside the CB frame and their calibration using both cosmic rays and test beam data is currently underway.

To cover the forward region the setup is completed by the TAPS calorimeter which is composed of 384 BaF_2 elements, each 25 cm in length (12 radiation lengths) and hexagonal in cross section, with a diameter of 59 mm. The front of every TAPS element is covered by a 5 mm thick plastic veto scintillator. The single counter time resolution is $\sigma_t = 0.2$ ns, the energy resolution can be described by $\Delta E/E = 0.018 + 0.008/E[GeV]^{0.5}$ [21]. The angular resolution in the polar angle is better than 1°, and in the azimuthal angle it improves with increasing θ, being always better than $1/R$ radian, where R is the distance in centimeters from the central point of the TAPS wall surface to the point on the surface where the particle trajectory meets the detector. The TAPS readout was custom built for the beginning of the CB@MAMI program and is effected in such a way as to allow particle identification by Pulse Shape Analysis (PSA), Time Of Flight (TOF) and $\Delta E/E$ methods (using the energy deposit in the plastic scintillator to give ΔE). TAPS can also contribute to the CB multiplicity trigger and is currrently divided into upto six sectors for this purpose. The 2 inner rings of 18 BaF_2 elements have been replaced recently by 72 $PbWO_4$ crystals each 20 cm in length (22 radiation lengths). The higher granularity improves the rate capability as well as the angular resolution. The crystals are operated at room temperature. The energy resolution for photons is similar to BaF_2 under these conditions [23].

References

[1] S. Capstick and C. Isgur, Phys. Rev. D **34**, 2809 (1986); S. Capstick and W. Roberts, Phys. Rev. D **49**, 4570 (1994).

[2] N. Kaiser, P.B. Siegel and W. Weise Phys. Lett. B **362**, 23 (1995).

[3] D. Jido, et al., Nucl. Phys. A **725** 181 (2003)

[4] M.F.M. Lutz and E.E. Kolomeitsev, Nucl. Phys. A 700 193 (2002)
J. Hofmann and M. F. M. Lutz, Nucl. Phys. A **776** 17 (2006)

[5] M. Doring, E. Oset, and D Strottman, Phys. Rev. C **73**, 045209 (2006).

[6] C. Amsler et al. [Particle Data Group], Phys. Lett. **B667**, 1 (2008).

[7] I. Horn, PhD thesis, Universität Bonn, Bonn (2004); I. Horn *et al.* [The CB-ELSA collaboration], Eur. Phys. J. A **38**, 173 (2008).

[8] M. Doring, E. Oset and D. Strottman, Int. J. Mod. Phys. A **22** (2007) 537.

[9] M. Doring, Nucl. Phys. A **786** (2007) 164

[10] M. Doring, E. Oset and D. Strottman, Phys. Lett. B **639** (2006) 59

[11] J. Ajaka *et al.*, Phys. Rev. Lett. **100**, 052003 (2008).

[12] V. L. Kashevarov *et al.*, arXiv:0901.3888 [hep-ex] (submitted to EPJA).

[13] Ch. Weinheimer *et al.*, Nucl. Phys. A **721**, 781c (2003).

[14] T. Nakabayashi *et al.*, Phys. Rev. C **74**, 035202 (2006).

[15] E. Gutz *et al.* [The CBELSA/TAPS Collaboration], Eur. Phys. J. A **35**, 291 (2008).

[16] A. Fix, M. Ostrick and L. Tiator, Eur. Phys. J. A **36**, 61 (2008).

[17] W. Roberts and T. Oed, Phys. Rev. C **71**, 055201 (2005) [arXiv:nucl-th/0410012].

[18] J.C. McGeorge et al.: Eur. Phys. J. **A 37** (2008) 129

[19] A. Reiter et al.: Eur. Phys. J. **A 30** (2006) 461

[20] A. Thomas et al.: Nucl. Phys. **B 79** (1999) 591

[21] S. Prakhov et al.: Phys. Rev. **C 79** (2009) 035204

[22] G. Audit et al.: Nucl. Instr. Meth. **A 301** (1991) 473

[23] R. Novotny *et al.*: Nucl. Instrum. Meth. A **486** (2002) 131